$(\vec{p},n)$ reaction on carbon isotopes at $E_p = 160$ MeV

J. Rapaport* and D. Wang
Ohio University, Athens, Ohio 45701

J. A. Carr† and F. Petrovich
Florida State University, Tallahassee, Florida 32306

C. C. Foster and C. D. Goodman
Indiana University, Bloomington, Indiana 47405

C. Gaarde and J. Larsen
Niels Bohr Institute, Copenhagen, Denmark

C. A. Goulding and T. N. Taddeucci
Los Alamos National Laboratory, Los Alamos, New Mexico 87545

D. Horen
Oak Ridge National Laboratory, Oak Ridge, Tennessee 37830

E. Sugarbaker
Ohio State University, Columbus, Ohio 43215
(Received 2 February 1987)

Differential cross sections and analyzing powers for the $(\vec{p},n)$ reaction on carbon isotopes have been measured for angles up to $\theta_{lab} = 50°$ using 160 MeV protons. The angular distributions for the stronger transitions are compared with the results of distorted-wave impulse approximation calculations which utilize transition densities from existing shell model calculations. The total observed Gamow-Teller strength is also compared with the shell model predictions. In addition, the shapes of these angular distributions are discussed emphasizing decomposition into longitudinal, transverse, and non-normal-parity-transfer components. Some comparisons of the present (p,n) data with corresponding (p,p') data and with other relevant (p,n) data are also made.

I. INTRODUCTION

In recent years, experimental studies of the (p,n) reaction at intermediate energies have provided new information on isovector modes of excitation in nuclei. Specifically, empirical proportionality factors have been used to relate 0° (p,n) cross sections to the Fermi (F) and Gamow-Teller (GT) strengths for the corresponding transitions.[1] Subsequently, studies of nuclides throughout the Periodic Table have established that the Gamow-Teller strength B(GT), integrated up to about 20 MeV excitation energy, is only a fraction of the strength estimated (in this same energy region) from nuclear structure calculations for light and medium mass nuclei or from the sum rule limit for heavy nuclei.[2] Complementary structure and reaction information can, in principle, be obtained from angular distributions of the differential cross section and other observables such as the analyzing power and polarization transfer coefficients. The motivation for examining such data in detail is becoming stronger as attention shifts from the low-momentum-transfer response so well characterized in the 0° GT studies to the response at larger momentum transfers.

Nuclides in the p shell, the isotopes of carbon in particular, are well suited for both GT strength distribution studies and extension of these structure studies to higher momentum transfers. The final states populated by GT-type (p,n) transitions are well separated and wave functions such as those of Cohen and Kurath[3] provide a reasonable first estimate of the transition densities needed for the comparison between theory and experiment. Differential cross sections for intermediate-energy ($E_p \geq 100$ MeV) ^{12,13,14}C(p,n) reactions have been studied by many investigators.[4–13] Recently, the results of 0° spin-flip probability measurements have also been reported.[10,11,14] In this paper we present differential cross section and analyzing power data for momentum transfers up to about 2 fm^{-1} for 160 MeV $(\vec{p},n)$ reactions on ^{12,13,14}C. The goal of the present study is to emphasize the important nuclear structure information that can be obtained from these data and to identify characteristics of the reactions that are not yet understood. For this reason we limit our analysis to several of the strongest GT transitions observed in these reactions.

II. EXPERIMENTAL METHOD

The experiment was performed using the beam swinger neutron time-of-flight facility at the Indiana University

TABLE I. Carbon target compositions.

Isotope	Total thickness (mg/cm^2)	Enrichment (%)
^{12}C	96.5	99.9
^{13}C	97.6	97
^{14}C	112	49 (92 mCi)

Cyclotron Facility (IUCF).[15] Polarized protons with an energy of 160 MeV were focused on isotopically enriched carbon targets. The polarization of the beam was periodically determined from measurements of simultaneous left-right scattering in a helium polarimeter located in the low-energy transfer beam line between the injector and main-stage cyclotrons. Typical values for the beam polarization ranged between 60% and 70%. During data acquisition, the spin orientation of the beam and the active data arrays were switched at 1 min intervals under automatic computer control. Large volume time-compensated plastic scintillators[16] were located at two neutron detector stations. One station was along the 0° beam line at 100 m flight path and the second station along the 24° line at a distance of 40 m. (Additional details about the experimental setup may be found in Ref. 15.) Data were obtained for an angular range $0° \leq \theta_{lab} < 50°$ with typical subnanosecond time resolution, which corresponds approximately to an energy resolution of 600 keV for the detector at 100 m. The electronics and data acquisition system used were similar to that described in Ref. 17.

Absolute cross section values were obtained with a normalization factor determined from neutron yields for the ^{7}Li(p,n)^{7}Be(g.s. +0.43 MeV) reaction measured under the same experimental conditions. The method has been described in detail in Ref. 4. A recent value[18] for the ^{7}Li(p,n)^{7}Be(g.s+0.43 MeV) total cross section was used to obtain the 0° differential cross section [$\sigma_{lab}(0°) = 37$ mb/sr] needed for this normalization procedure. This new total cross section value is about 13% smaller than the value (for $E_p = 160$ MeV) upon which previous normalizations were based,[8,9] so these previous cross section values[8,9] need to be multiplied by 0.87 to be consistent with the present measurements.

The thicknesses and enrichments of the self-supported carbon targets are given in Table I. The ^{14}C material was obtained in a fine powder form and mixed with a small amount of ^{12}C. This mixture was pressed into a solid disk and enclosed between thin styrene films as a safety precaution.

III. DATA AND RESULTS

Differential cross sections and analyzing powers were measured over the entire angular range of $0° \leq \theta_{lab} < 50°$. The forward angle cross section data were used to extrapolate the cross section to zero momentum transfer and make a suitable comparison with B(GT) values determined from beta-decay lifetimes. At larger angles the analyzing power becomes significant and the differential cross section distributions exhibit differences in shape. These features provide additional information on the structure of the state. In the next few paragraphs we will present the data and theoretical results obtained for the strongest transitions in each carbon isotope.

A. The ^{12}C(p,n)^{12}N reaction

A 0° spectrum for this reaction (c.m. differential cross section versus outgoing neutron energy) is presented in the top part of Fig. 1. The measured differential cross section and analyzing power distributions for the 1^+, $T = 1$ ^{12}N(g.s.) transition are presented versus momentum transfer in Fig. 2. In the same figure, data for the ^{12}C(p,p')^{12}C(1^+ $T = 1$, 15.11 MeV) reaction at $E_p = 190$ MeV (Ref. 19) are also shown. Isospin conservation implies that the cross section for the ^{12}C(p,n)^{12}N(g.s.) reaction should be twice as large as the cross section for the analog ^{12}C(p,p')^{12}C(15.11 MeV) reaction at the same incident energy.[20] Twice the measured values for the (p,p') cross sections are presented in Fig. 2. Because the spin-isospin term of the effective nucleon-nucleon interaction at energies between 120 and 200 MeV is almost energy independent[8] and differences in (p,p') and (p,n) distortion effects are small at these energies,[21–23] the differential cross section and analyzing power distributions for these two reactions are expected to be similar. By superimposing the (p,p') and (p,n) data in this manner, we make this

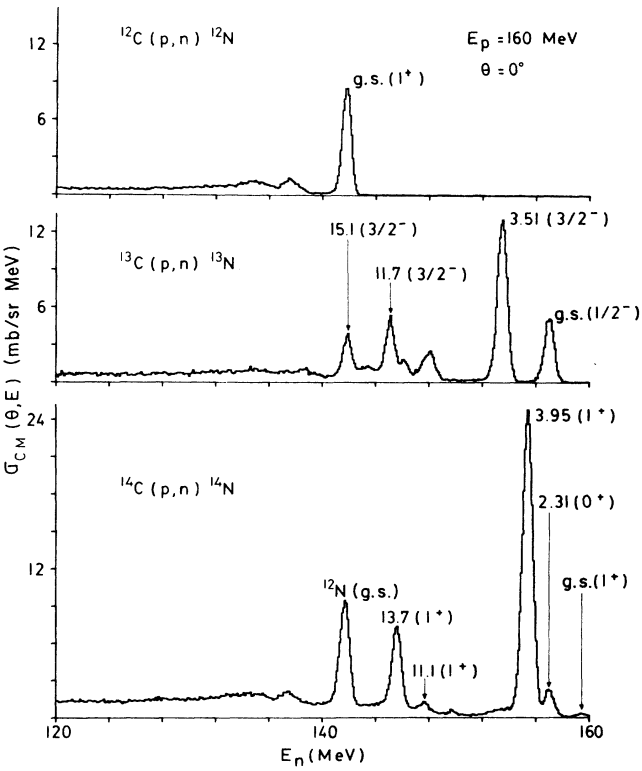

FIG. 1. Excitation energy spectra for (p,n) reactions on carbon isotopes at $E_p = 160$ MeV and $\theta = 0°$.

comparison in Fig. 2. The differential cross section distributions show the expected similarity; the analyzing power distributions (which are more sensitive to small amplitudes) exhibit significant differences for $q \geq 0.7$ fm^{-1}.

The curves shown in Fig. 2 are distorted wave impulse approximation (DWIA) results for the ^{12}C(p,n)^{12}N(g.s.) reaction at $E_p = 160$ MeV, carried out with the code DWBA70.[24] The optical model potential (OMP) parameters used in these calculations are from Ref. 25, and the effective interaction used was the 175-MeV parametrization of Franey and Love.[26] Spectroscopic amplitudes for the ^{12}C(p,n)^{12}N(g.s.) $0^+ \rightarrow 1^+$ transition were obtained from shell model calculations employing the effective $1p$-shell interaction of Cohen and Kurath (CKWF).[3] These wave functions are known to give a reasonable description of the electromagnetic and beta decay rates for this transition.[3] Harmonic oscillator radial wave functions were used for the single-particle states. The oscillator range parameter $b = 1.87$ fm was the same one used in previous studies,[19,27] a choice that fits the prominent maxima of the transverse form factors obtained from (e,e′) experiments but deviates appreciably from the electron scattering data for $q > 1.3$ fm^{-1}. The present theoretical (p,n) results are likewise expected to be inadequate beyond this momentum transfer. The solid curves in Fig. 2 correspond to calculations with the full CKWF. Results are also shown (dashed curves) with the non-normal parity $[LSJ] = [111]$ transition amplitudes excluded from the calculations. This has an important effect on the analyzing power values and the differential cross section (in the region of the first maximum and beyond) and will be discussed further in Secs. IV C and IV D.

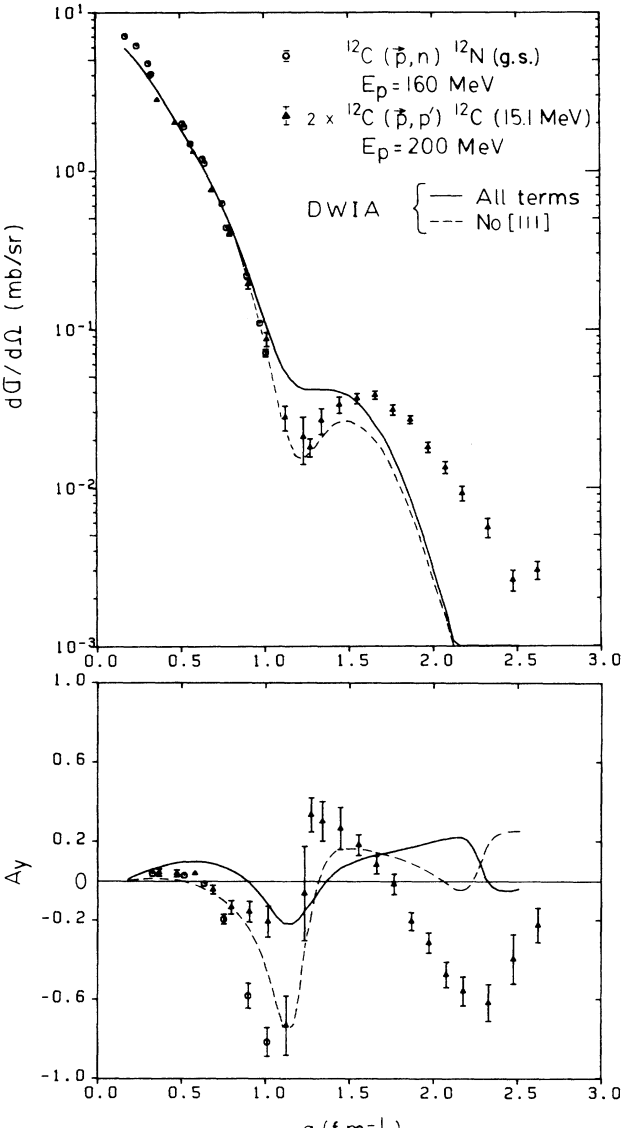

FIG. 2. Differential cross section and analyzing powers for the ^{12}C($\vec{p}$,n)^{12}N(g.s.) transition at $E_p = 160$ MeV (circles). Analyzing powers and twice the differential cross section values for the ^{12}C($\vec{p}$,p′)^{12}C(15.19 MeV) transition at $E_p = 200$ MeV from Ref. 19 are also shown (triangles). The solid curves are the theoretical result obtained with the CKWF and the dashed curves are the results obtained with the non-normal parity $[LSJ] = [111]$ target density excluded. See discussion in Secs. IV C and IV D.

B. The ^{13}C(p,n)^{13}N reaction

Differential cross section and transverse spin-flip probability data for this reaction at $\theta = 0°$ and $E_p = 160$ MeV have been previously reported in Ref. 11. A 0° spectrum of differential cross section versus neutron energy for the ^{13}C(p,n)^{13}N reaction is presented in the middle of Fig. 1. The measured differential cross section and analyzing power distributions for the g.s. and 3.51 MeV transitions are presented versus momentum transfer in Fig. 3.

The g.s. mirror transition ^{13}C($\frac{1}{2}^-$)$\rightarrow$^{13}N($\frac{1}{2}^-$) proceeds via an incoherent mixture of Fermi and Gamow-Teller amplitudes. The ^{13}C(g.s., $\frac{1}{2}^-$)$\rightarrow$^{13}N(3.51 MeV, $\frac{3}{2}^-$) transition proceeds via an incoherent mixture of Gamow-Teller and quadrupole amplitudes. The curves in Fig. 3 represent DWIA calculations using CKWF (Ref. 3) for the corresponding transitions and an oscillator range parameter $b = 1.82$ fm. The solid curves represent the summed differential cross sections and the individual contributions to each transition are shown as labeled. The DWIA calculations were done in the same fashion as those described in the preceding section for the ^{12}C(p,n)^{12}N(g.s.) transition. The theoretical $\Delta J^\pi = 1^+$ contribution to the differential cross section for the 3.51-MeV excitation has been scaled by a factor of 0.52 (see Sec. IV A). The need for a large correction to results obtained with the CKWF (Ref. 3) for the $\frac{1}{2}^- \rightarrow \frac{3}{2}^-$ transition in ^{13}C(p,n) has been noted in the spin-transfer work[11] and work on the energy dependence of the $J_{\sigma\tau}/J_\tau$ ratio.[28] Related considerations for the $\frac{1}{2}^- \rightarrow \frac{1}{2}^-$ transition and an anomaly in the absolute (p,n) cross sections for light odd-A targets have also been discussed recently.[29] We address the question of the normalization of the various contributions to the ^{13}C(p,n) cross sections and the comparison with beta decay and the even carbon isotopes in some detail in Sec. IV A. Finally, we note that the shape of the distribution for the g.s. transition, unlike that for the

3.51-MeV state, is not very well reproduced by the calculations for momentum transfer $q \geq 0.7$ fm^{-1}. The shapes of the differential cross section distributions will be discussed in more detail in Sec. IV C.

C. The ^{14}C(p,n)^{14}N reaction

A 0° spectrum for this reaction is presented in the bottom of Fig. 1. Differential cross section and analyzing power distributions for transitions to the $J^\pi = 0^+$ ($E_x = 2.31$ MeV) isobaric analog (IA) state and to the $J^\pi = 1^+$ ($E_x = 3.95$ MeV) state are shown in Fig. 4.

The solid curves in Fig. 4 are DWIA calculations using CKWF (Ref. 3) for the corresponding transitions. An oscillator parameter value of $b = 2.0$ fm was used in these calculations. The $\Delta J^\pi = 1^+$ result for the 3.95 MeV excitation has been multiplied by 0.6. This renormalization is expected from comparison to beta decay and is discussed further in Sec. IV A. In addition, we note that a better description of the IA transition is obtained by using $b = 2.32$ fm and scaling the result by 0.8. This result is indicated by the dashed curve in Fig. 4. The need for a different oscillator constant for the Fermi and Gamow-Teller transitions could easily be a reflection of true differences in the radial transition densities for these transitions or an effect of expected density dependence in the t_τ component of the effective interaction.[23]

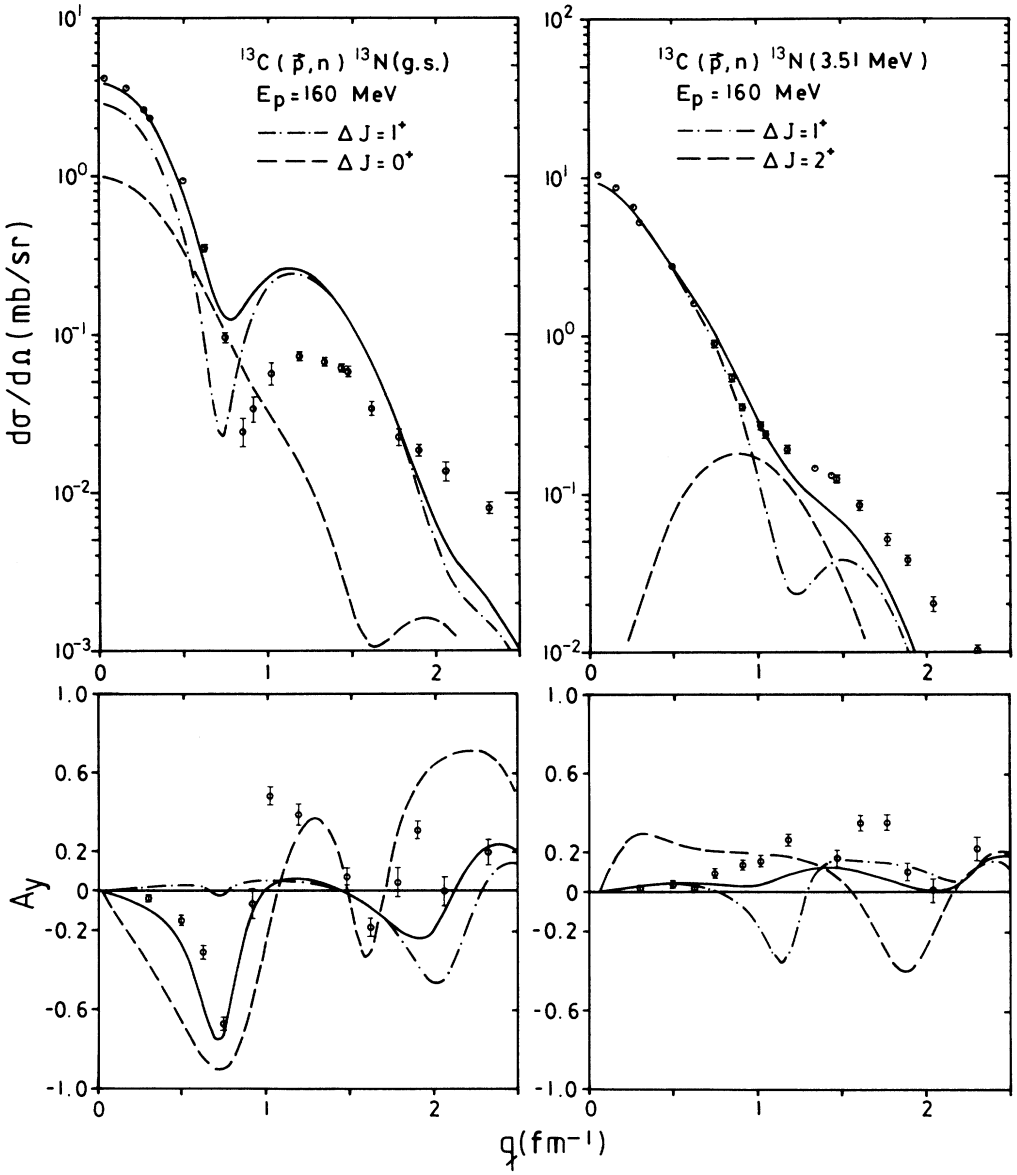

FIG. 3. Differential cross section and analyzing powers for ^{13}C(p⃗,n)^{13}N(g.s., and 3.51 MeV) transitions at $E_p = 160$ MeV. The curves are DWIA results using CKWF. The separate ΔJ^π contributions are shown as dashed and dotted-dashed curves and the solid curves represent the incoherent sum of the component cross sections. The $\Delta J^\pi = 1^+$ DWIA result for the 3.52 MeV excitation has been multiplied by 0.52. See Sec. IV A.

IV. DISCUSSION

The results in the preceding section have a number of common features which we have chosen to discuss collectively in this section.

We have four points to make. We first relate the normalization of the theoretical and experimental differential cross sections to existing beta-decay data and compare these normalizations to the large body of such values for (p,n) reactions on other nuclei.

These normalizations are then used to obtain the B(GT) value for the transition to the 3.51 MeV state in ^{13}N. In subsection B we examine the quenching of the Gamow-Teller strength. Next, we discuss the origin of the similarities and differences noted in the shapes of the angular distributions shown in Figs. 2–4. These are seen to provide information on the longitudinal spin dipole transition density. In subsection D we extend this discussion to include the information contained in the analyzing power data.

A. Normalization of the differential cross sections

Experimental ft values are available[30,31] for allowed beta-decay transitions in the carbon isotopes corresponding to four of the five (p,n) transitions discussed in Sec.

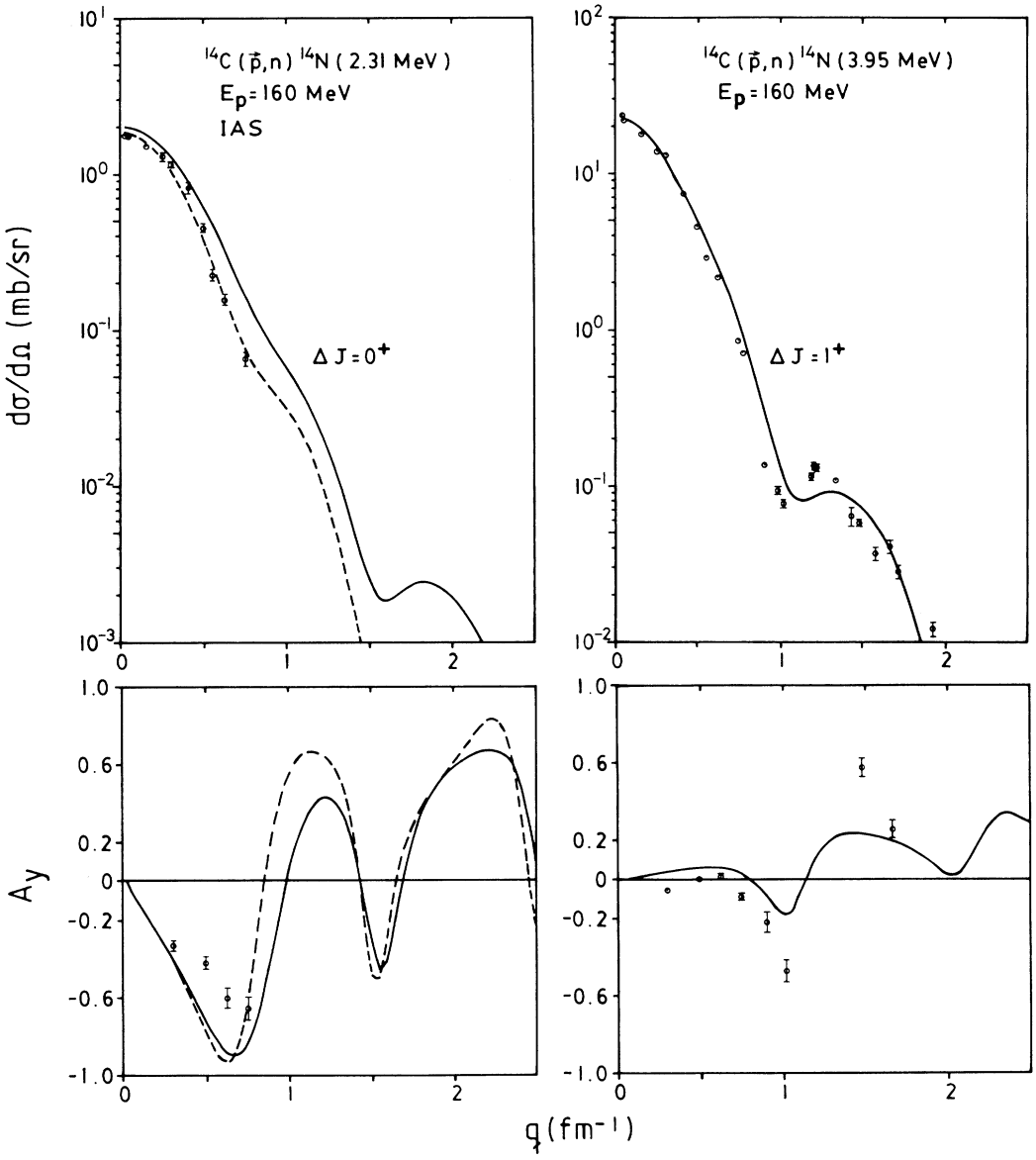

FIG. 4. Differential cross section and analyzing powers for the ^{14}C($\vec{p}$,n)^{14}N(2.31 MeV and 3.95 MeV) transitions at $E_p = 160$ MeV. The curves are DWIA calculations using CKWF. The solid curves are obtained with an oscillator range parameter $b = 2.0$ fm^{-1}. The $\Delta J = 1^+$ result for the 3.95-MeV excitation has been multiplied by 0.6. The dashed curve for the IA transition is calculated with $b = 2.2$ fm^{-1} and has been multiplied by 0.8. See Sec. IV A.

III. Beta decay transition strengths have been obtained from these ft values using the coupling constant values recommended by Wilkinson.[32] An additional ft value is available for the transition corresponding to the $\frac{1}{2}^-, T=\frac{1}{2} \rightarrow \frac{3}{2}^- T=\frac{3}{2}$ ^{13}C(p,n)^{13}N(15.1 MeV) reaction. These experimental transition strengths are compared with CKWF predictions in Table II. Also included in the table are estimated transition strengths for the ^{13}C(p,n)^{13}N(3.51 MeV) $\frac{1}{2}^-, T=\frac{1}{2} \rightarrow \frac{3}{2}^-, T=\frac{1}{2}$ reaction and for the ^{15}N(p,n)^{15}O(6.18 MeV) $\frac{1}{2}^-, T=\frac{1}{2} \rightarrow \frac{3}{2}^-, T=\frac{1}{2}$ reaction as well as the known beta decay strength for the mirror ^{15}N(p,n)^{15}O(g.s.) transition. These transitions will be discussed below.

The ratios of the experimental beta-decay transition strengths to those given by the CKWF for the GT transition in mass 12 and the Fermi and GT transitions in mass 14 are 0.98, 1.0, and 0.57, respectively. This roughly accounts for the normalization of the theoretical results presented in Figs. 2 and 4 and suggests that the strengths of the t_τ and $t_{\sigma\tau}$ components of the t-matrix interaction of Ref. 26 are consistent with these particular experimental cross sections. The ratio of the experimental beta-decay transition strengths to those of CKWF for the Fermi and GT components of the $\frac{1}{2}^- \rightarrow \frac{1}{2}^-$ ground state mirror transition in mass 13 are 1.0 and 0.62, respectively. The theoretical differential cross section for this transition shown in Fig. 3 is slightly below the experimental data at 0°. If just the $\Delta J^\pi = 1^+$ contribution is reduced by a factor 0.62 as the beta-decay data suggest, the resulting summed theoretical cross section at $\theta = 0°$ is 2.9 mb/sr or about 69% of the experimental value. Essentially identical results are obtained for the $T=\frac{3}{2}$ ($E_x = 15.1$ MeV) excitation in the ^{13}C(p,n)^{13}N reaction (not shown).[29] We conclude that there is an unexpected difference in the ratio of (p,n) cross section to beta decay transition strength for the even and odd carbon isotopes. This difference is not peculiar to the (p,n) reaction. Differential cross sections have been reported for the ^{13}C(p,p′)^{13}C(15.1 MeV, $T=\frac{3}{2}$) reaction at 135 MeV by Collins *et al.*,[33] and the ^{12}C(p,p′)^{12}C(15.1 MeV, $T=1$) reaction has been studied at the same incident energy by these authors,[34] and by Comfort *et al.*[27] at 120 MeV. The (p,p′) differential cross section (at the same momentum transfer) per unit B(GT) is at least a factor of 2 larger for ^{13}C than for ^{12}C. Similar discrepancies have been noted for (p,n) reactions on even and odd Li targets and also in ^{15}N and ^{35}K. These have been discussed in some detail recently by Taddeucci *et al.*[29]

One possible explanation for these anomalies might be distortion effects associated with possible differences in optical potentials for even and odd isotopes for which no detailed studies have been made. As in the present study, distortion effects in the (p,n) reaction have been estimated using optical potentials obtained from elastic scattering from abundant even-A isotopes. A preliminary study was done by searching on OMP parameters with the 200 MeV proton elastic differential cross section and analyzing power data on ^{12,13}C reported by Meyer *et al.*[35] Spherical OMP parameters and coupled channels potential parameters were obtained. With these sets of parameters distortion factors were calculated for the (p,n) reactions. However, the anomaly indicated above still persisted. Another possibility is that there are important differences in channel coupling effects in the even and odd systems. Again, no definitive work has been done on this problem. However, recent ^{12,13}C(p,n) data reported for $E_p = 800$ MeV (Ref. 13) seem to indicate that the discrepancy has vanished at this energy. This would point toward possible channel effects that would become less important at higher energies. The answers to these questions must await future studies. The main point to be made here is that the discrepancy between ^{12,14}C and ^{13}C noted above appears to be an *overall* normalization effect, i.e., consistent results for the 0° cross sections for the g.s. mirror transition and the $T=\frac{3}{2}$ excitation in mass 13 are obtained by first scaling to the beta-decay data and multiplying the final results by a factor of 1.5 relative to ^{12,14}C. This factor is the ratio of the weighted average values of

TABLE II. Structure information on transitions studied with (p,n) reactions at $E_p = 160$ MeV.

Target	J_i^π, T_i	J_f^π, T_f	E_x (MeV)	B(GT) Expt.	B(GT) CKWF	$B(F)$	$\hat{\sigma}_{GT}$[c] (mb/sr)	$\hat{\sigma}_F$[c] (mb/sr)
^{12}C	$0^+,0$	$1^+,1$	0.0	0.90 ±0.01[a]	0.92	0	8.8	0
^{13}C	$\frac{1}{2}^-,\frac{1}{2}$	$\frac{1}{2}^-,\frac{1}{2}$	0.0	0.200±0.004[a]	0.323	1	12.8	1.55
		$\frac{3}{2}^-,\frac{1}{2}$	3.51	0.83 ±0.03[b]	2.38	0		0
		$\frac{3}{2}^-,\frac{3}{2}$	15.1	0.23 ±0.01[d]	0.316	0	13.8	0
^{14}C	$0^+,1$	$0^+,1$	2.31	0	0	2	0	0.92
		$1^+,0$	3.95	2.76 ±0.11[a]	4.84	0	8.4	0
^{15}N	$\frac{1}{2}^-,\frac{1}{2}$	$\frac{1}{2}^-,\frac{1}{2}$	0.0	0.256±0.004[a]	0.333	1	12.4	1.41
		$\frac{3}{2}^-,\frac{1}{2}$	6.18	1.0 ±0.1[b]	2.667	0		0

[a] Values obtained from beta decay lifetimes (Refs. 30 and 31).
[b] Estimates from 0° (p,n) cross sections. See text.
[c] Cross section per unit B(GT) and $B(F)$ at momentum transfer $q=0$. Estimated uncertainty ±10%.
[d] Value obtained considering rate asymmetry for mirror decays. (See Ref. 29 for a discussion of this point.)

$\hat{\sigma}_{GT}$ for ^{13}C to those for ^{12,14}C (Table II). A similar factor is obtained for the ratio of $\hat{\sigma}_F$ (Table II). This means that the Gamow-Teller strength distributions can be obtained with confidence for each nucleus, but a precise understanding of the actual cross section magnitudes is presently lacking.

To quantify our results and provide a factor to convert 160 MeV C(p,n) cross sections to beta-decay transition strengths B(GT), we use the experimental cross section data and beta-decay strength for the transitions being discussed to arrive at the conversion factors $\hat{\sigma}_{GT}$ and $\hat{\sigma}_F$ in Table II. These empirical factors are the so-called "unit cross sections" defined and discussed by Taddeucci *et al.*[29] and represent the cross section per unit GT or F transition strengths at $q=0$. In all cases the measured 0° (p,n) cross sections have been extrapolated to their corresponding values at zero momentum transfer[29] before conversion to beta-decay transition strength. Following this procedure we obtain $B(\mathrm{GT})=0.83\pm0.03$ for the ^{13}C(p,n)^{13}N transition to the 3.51 MeV state as indicated in Table II. As mentioned earlier, this result is consistent with our earlier work on spin transfer[11] and the energy dependence of $J_{\sigma\tau}/J_{\tau}$.[28] The ratio $B(\mathrm{GT})_{\mathrm{expt}}/B(\mathrm{GT})_{\mathrm{CKWF}}=0.35$ multiplied by 1.5 gives the normalization factor of 0.52 used in Fig. 3.

In Fig. 5 we present a reconstruction of Fig. 3 for the transitions studied in mass 13 with the theoretical curves normalized according to the above discussion. The

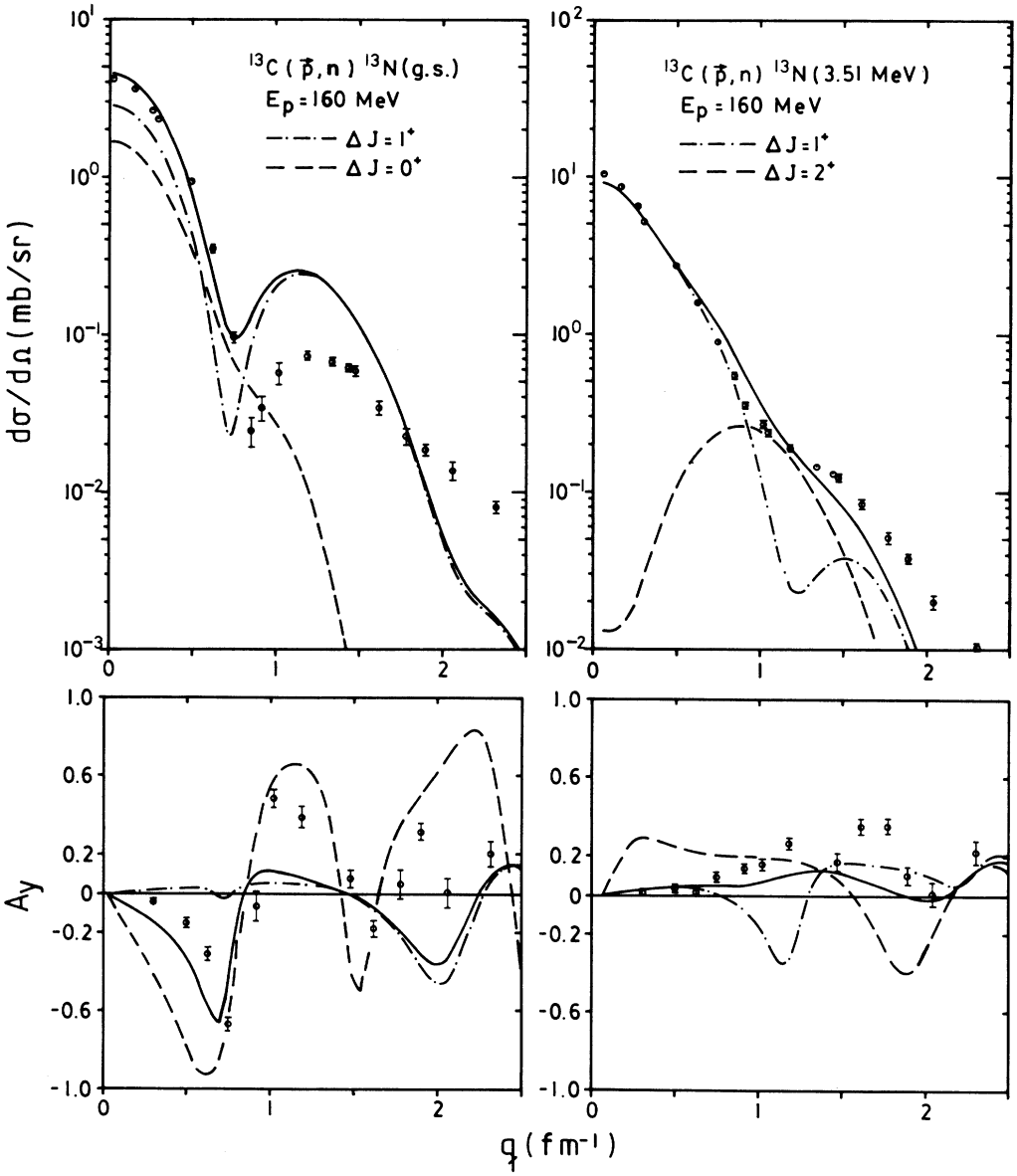

FIG. 5. Experimental results for the ^{13}C(p⃗,n)^{13}N reaction compared to DWIA curves that have been renormalized as indicated in Sec. IV A.

$\Delta J^\pi = 0^+$ contribution to the g.s. differential cross section shown in Fig. 5 has been calculated with an oscillator parameter $b = 2.32$ fm and multiplied by 0.8; these values are suggested by the comparison to the ^{14}C IAS (isobaric analog state) transition shown by the dashed curve in Fig. 4. The relative $\Delta J^\pi = 1^+$ and $\Delta J^\pi = 0^+$ contributions to the cross section for the g.s. mirror transition at $\theta = 0°$ are different in Figs. 3 and 5. The ratio of these contributions is approximately 3/1 in Fig. 3 and is reduced to $2.9/1.5 = 1.9$ in Fig. 5. The ratio of these cross sections predicted from the empirical value of $J_{\sigma\tau}/J_\tau$ reported in Refs. 28 and 29 is 1.9 and in excellent agreement with the values of Fig. 5. There is also very good agreement with the spin-transfer results of Ref. 11. The theoretical results presented in Fig. 3 do not show this same level of consistency.

Overall, the shape of the theoretical cross section distribution for the $\frac{1}{2}^- \rightarrow \frac{1}{2}^-$ g.s. transition is only slightly improved relative to the data by the different treatment of the normalization and the Fermi amplitude. The only difference in the results of Figs. 3 and 5 for the 3.51-MeV excitation is in the magnitude of the $\Delta J^\pi = 2^+$ contribution to the differential cross section. The results in Fig. 5, in the context of the stated normalization procedure, indicate the $\Delta J^\pi = 2^+$ contribution at the full CKWF value. The results in Fig. 3 show the $\Delta J^\pi = 2^+$ contribution reduced by a factor of 1.5 relative to the $\Delta J^\pi = 1^+$ contribution.

B. Total Gamow-Teller strength

Excitation energies and transition strengths for all the GT transitions are available from the CKWF.[3] These predictions are compared with the empirical GT strength distributions from the present work in Fig. 6. The experimental strengths were obtained with the empirical conversion factors given in Table II. The calculated excitation energies of the GT transitions are in general agreement with the empirical GT distribution for all three carbon isotopes. As indicated above, there is good agreement between calculated and experimental GT strength for the ^{12}C(p,n)^{12}N(g.s.) transition (Table II). In the case of ^{13}C the calculated GT strengths are larger than experimentally determined values, particularly for the ^{13}C(p,n)^{13}N(3.51 MeV) transition where the CKWF give a value almost 3 times larger than the empirical value.[11] The total measured strength (up to 16 MeV excitation energy in ^{13}N) is $\sum B(\mathrm{GT}) = 1.8$, while the summed CKWF strength, up to roughly the same excitation energy, is 3.95. Defining a GT quenching factor Q_{GT} to be the ratio between experimental and calculated GT strength, the value $Q_{\mathrm{GT}} = 0.46$ is obtained for the ^{13}C(p,n)^{13}N reaction. This is rather low, but is similar to the value obtained for the ^{15}N(p,n)^{15}O reaction.[11] For ^{14}C the observed total strength is about 60% of the CKWF value of 6.0. The value $Q_{\mathrm{GT}} = 0.6$ obtained for ^{14}C(p,n)^{14}N is closer to global values reported for many other nuclei.[2] The difficulties with the overall distribution of strength is an indicator that the simple truncation of the model space assumed by the CKWF (Ref. 3) is not a good approximation for 1p-shell nuclei near the end of the shell.

C. Shapes of the differential cross section distributions

The overall shapes of the $\Delta J^\pi = 1^+$ contributions to the ^{12,13,14}C(p,n) differential cross section distributions, except for the forward peaking, are not sharply characterized by the angular momentum transfer, unlike the situation familiar from many inelastic nucleon scattering studies on natural parity excitations.[23] The most striking example of this in the present work is the difference in the shape of

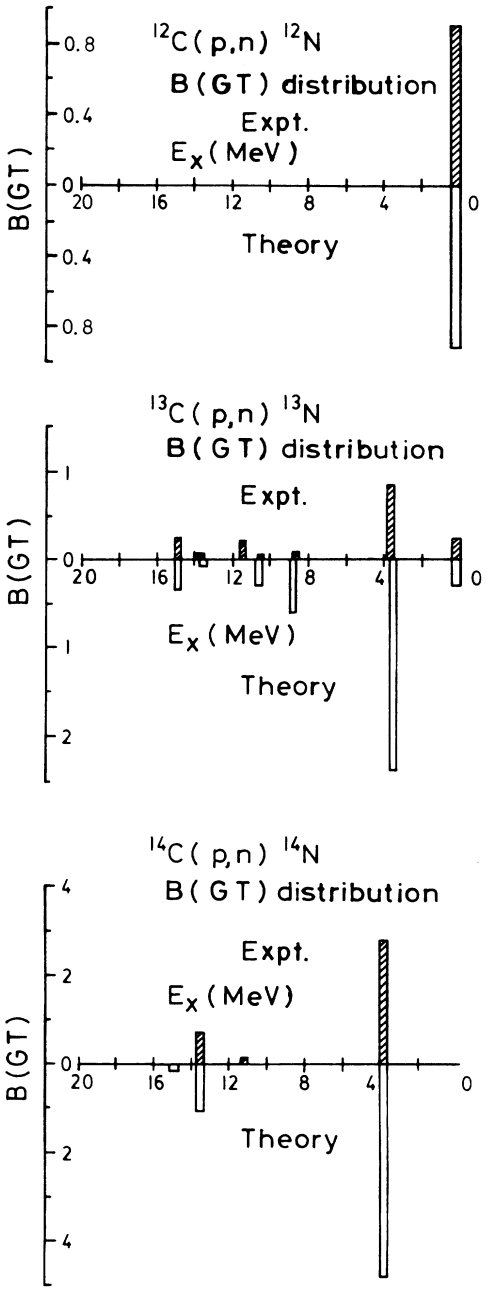

FIG. 6. Experimental and calculated (CKWF) GT strength distributions for the carbon isotopes.

the cross-section distributions for the first two excitations in ^{13}C(p,n)^{13}N shown in Figs. 3 and 5. The absence of a sharply characteristic shape for $\Delta J^\pi = 1^+$ differential cross section distributions is a general feature of unnatural-parity transitions in contrast to natural parity transitions. To illustrate this we note, specializing to the cases of $\Delta J^\pi = 0^+$ and $\Delta J^\pi = 1^+$ transitions in the (p,n) reaction, that the plane wave differential cross sections at zero energy transfer are given to a good approximation by[36,37]

$$\left[\frac{d\sigma}{d\Omega}\right]_{0^+} \simeq 8\pi \left[\frac{\mu}{2\pi\hbar^2}\right]^2 |\,\bar{t}^{\,1}_m(q,k_{\text{c.m.}})\rho^m_{01}(q)\,|^2 , \quad (1)$$

$$\left[\frac{d\sigma}{d\Omega}\right]_{1^+} \simeq 8\pi \left[\frac{\mu}{2\pi\hbar^2}\right]^2 \frac{2J_f+1}{2J_i+1} \times [\,|\,\bar{t}^{\,1}_{s\parallel}(q,k_{\text{c.m.}})\rho^{s\parallel}_{11}(q)\,|^2 + |\,\bar{t}^{\,1}_{s\perp}(q,k_{\text{c.m.}})\rho^{s\perp}_{11}(q)\,|^2] , \quad (2)$$

where $\bar{t}^{\,1}_m$, $\bar{t}^{\,1}_{s\parallel}$, and $\bar{t}^{\,1}_{s\perp}$ are isovector "interaction" components that represent the coupling of the scattered nucleons to the isovector spherical mass transition density ρ^m_{01} ($\Delta J^\pi = 0^+$) and the isovector longitudinal and transverse spin dipole transition densities $\rho^{s\parallel}_{11}$ and $\rho^{s\perp}_{11}$ ($\Delta J^\pi = 1^+$) of the target nucleus, respectively. It is sufficient to consider plane wave results for the present purpose because distortion effects mainly reduce the plane wave cross sections by an overall factor of about 2 for light targets at the incident energies of interest.[29] In writing Eqs. (1) and (2) we have assumed a static local nucleon-nucleon effective interaction with central and tensor components as in the convention of Franey and Love.[26] (The isovector spin-orbit interaction is known to play only a small role in $\Delta J^\pi = 0^+$ and 1^+ transitions at the incident energies of interest here.[26]) In addition, we have made an approximation in treating the exchange integrals that excludes any coupling to current and spin-current distributions in either the projectile or target space.[38] The $[LSJ]=[111]$ non-normal parity transition densities referred to in Sec. III A are one particular class of these spin-current distributions.

The $\bar{t}$-matrix "interaction" components in Eqs. (1) and (2) are easily expressed in terms of the more familiar central (C) and tensor (T) components of the effective nucleon-nucleon interaction

$$\bar{t}^{\,1}_m(q,k_{\text{c.m.}}) = \bar{t}^{\,C}_\tau(q,k_{\text{c.m.}}) , \quad (3)$$

$$\bar{t}^{\,1}_{s\parallel}(q,k_{\text{c.m.}}) = \bar{t}^{\,C}_{\sigma\tau}(q,k_{\text{c.m.}}) = 2\bar{t}^{\,T}_\tau(q,k_{\text{c.m.}}) , \quad (4)$$

$$\bar{t}^{\,1}_{s\perp}(q,k_{\text{c.m.}}) = \bar{t}^{\,C}_{\sigma\tau}(q,k_{\text{c.m.}}) + \bar{t}^{\,T}_\tau(q,k_{\text{c.m.}}) , \quad (5)$$

where

$$\bar{t}^{\,C}(q,k_{\text{c.m.}}) = t^{C,D}(q) + t^{C,E}(k_{\text{c.m.}}) , \quad (6)$$

$$\bar{t}^{\,T}(q,k_{\text{c.m.}}) = t^{T,D}(q) - \tfrac{1}{2}t^{T,E}(k_{\text{c.m.}}) , \quad (7)$$

with D and E referring to direct and exchange and $k_{\text{c.m.}}$ representing the incident nucleon momentum in the nucleon-nucleus center of mass. The isovector longitudinal and transverse spin dipole transition densities are likewise easily expressed in terms of the more usual $L=0$ and 2 isovector spin dipole transition densities ρ^{s1}_{10} and ρ^{s1}_{12}:

$$\rho^{s\parallel}_{11} = \left[\frac{J}{2J+1}\right]^{1/2}\rho^{s1}_{10} + \left[\frac{J+1}{2J+1}\right]^{1/2}\rho^{s1}_{12} , \quad (8)$$

$$\rho^{s\perp}_{11} = \left[\frac{J+1}{2J+1}\right]^{1/2}\rho^{s1}_{10} - \left[\frac{J}{2J+1}\right]^{1/2}\rho^{s1}_{12} . \quad (9)$$

We also have the following connections between the transition densities and beta-decay matrix elements:

$$B(F) = 2\pi\,|\,\rho^m_{01}(0)\,|^2 , \quad (10)$$

$$B(\text{GT}) = 2\pi\frac{2J_f+1}{2J_i+1}\,|\,\rho^{s1}_{10}(0)\,|^2 . \quad (11)$$

The main point to be made about these relations is that the $\Delta J^\pi = 0^+$ natural parity cross section depends on a single interaction component and a single transition density while the $\Delta J^\pi = 1^+$ unnatural parity cross section depends on two interaction components and two transition densities. It is well known and has been discussed in detail elsewhere[37,39,40] that $\bar{t}^{\,1}_{s\parallel}$ and $\bar{t}^{\,1}_{s\perp}$ are driven by the π- and ρ-exchange mechanisms in the nucleon-nucleon interaction and consequently exhibit quite different q dependence. The shapes of the $\Delta J^\pi = 1^+$ differential cross section distributions thus depend sensitively on the relative values of $\rho^{s\parallel}_{11}$ and $\rho^{s\perp}_{11}$ for a particular transition. The latter, in turn, are sensitive to the shell-model structure of the state. This argument could also be made in terms of the central and tensor interaction components and the $L=0,2$ spin densities. The resulting cross section expressions contain interference terms, however, and one loses the direct connection to π and ρ exchange.

To be more explicit, we present in Fig. 7 approximate plane wave results based on Eq. (2) for the $\Delta J^\pi = 1^+$ contributions corresponding to the C(p,n) differential cross sections shown in Figs. 2–5. Also included in the figure are $\Delta J^\pi = 1^+$ results for the two transitions in ^{15}N(p,n) introduced in Table II. In each case the $\Delta J^\pi = 1^+$ cross section is decomposed into its transverse and longitudinal components. The interaction and nuclear structure input for the C(p,n) calculations of Fig. 7 are the same as for the calculations presented in Figs. 2–5. For the ^{15}N(p,n) calculations we have used CKWF (Ref. 3) with an oscillator size parameter $b = 1.82$ fm. No normalization factors have been applied to the results in Fig. 7. We have also made plane wave calculations with an exact treatment of the exchange integrals following the approach of Ref. 38. Equivalently, these results could have been obtained with the code DWBA70.[24] We find that the results of the approximate and exact plane wave calculations are in agreement to a few percent, except for contributions associated with non-normal parity $[LSJ]=[111]$ target densities which enter particularly strongly only in the case of ^{12}C. These $[LSJ]$ contributions to the plane wave cross sections are shown separately in Fig. 7. These contributions have not been included in the total $\Delta J^\pi = 1^+$ curves shown. The [111] contributions for ^{13}C(p,n) are essentially zero.

The strengths of the longitudinal and transverse in-

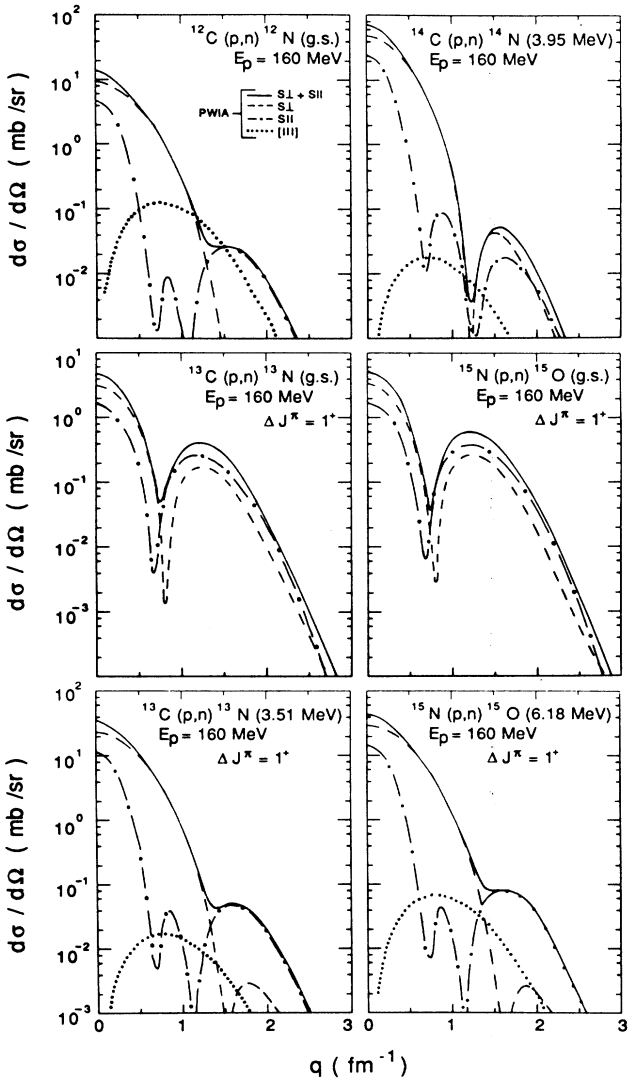

FIG. 7. Approximate plane wave results for $\Delta J^\pi = 1^+$ contributions to ^{12,13,14}C(p,n) and ^{15}N(p,n) differential cross sections. The complete differential cross sections are decomposed into transverse (dashed curve) and longitudinal (dotted-dashed curves) components. The contributions to the cross sections associated with $[LSJ]=[111]$ target densities are shown by the dotted curves. These are not included in the solid curves.

teractions are almost the same at $q=0$ in the energy region near $E_p \simeq 160$ MeV. This may be seen in Figs. 4 and 6 of Ref. 37. The longitudinal interaction drops off rapidly with increasing q, passing through zero at $q \simeq 0.7$ fm^{-1}. This rapid variation in q is characteristic of the long range π-exchange process. The transverse interaction decreases only slowly with increasing q, characteristic of the short range ρ-exchange process, and does not reach a minimum until $q \simeq 2.6$ fm^{-1}. The strength of the longitudinal interaction becomes comparable in magnitude to the transverse interaction at $q \simeq 1.5$ fm^{-1} and exceeds the latter for q beyond this value. The dominance of the longitudinal interaction component for $q \geq 1.5$ fm^{-1} explains the connection between past interest in the behavior of $\Delta J^\pi = 1^+$ nucleon scattering cross sections in this momentum transfer region and the question of precursors to pion condensation.[40] These features of the transverse and longitudinal interaction components are quite clear in the cross section results of Fig. 7. In particular, the longitudinal cross section is always small in the region $0.4 \leq q \leq 1.2$ fm^{-1}.

A complete understanding of the $\Delta J^\pi = 1^+$ differential cross sections in Fig. 7 requires consideration of the transition densities as well as the interaction components. In the p shell there are two distinct extremes. One is that the $L=0,2$ transition densities have the same sign at low q with magnitudes such that the longitudinal transition density [sum of $L=0$ and 2, Eq. (8)] has a minimum at large q and the transverse density [difference of $L=0$ and 2, Eq. (9)] has a minimum at low q. This is the situation for the $\frac{1}{2}^- \rightarrow \frac{1}{2}^-$ g.s. transitions in masses 13 and 15. The differential cross sections in these cases have minima at $q \simeq 0.8$ fm^{-1} because both $\bar{t}^1_{s\|}$ and $\rho^{s\perp}_\|$ have minima in this region. The other extreme is that $L=0$ and 2 start out with opposite signs at low q with magnitudes leading to the reverse situation of transverse and longitudinal transition densities having minima at high and low q, respectively. This is the circumstance for the $\frac{1}{2}^- \rightarrow \frac{3}{2}^-$ transitions in mass 13 and 15 and the $0^+ \rightarrow 1^+$ transition in ^{12}C which is dominated by the $p_{3/2} \rightarrow p_{1/2}$ single particle matrix element. The differential cross sections for these transitions have minima at $q \simeq 1.3$ fm^{-1}. These cross section minima are not associated with minima in the transition densities or interaction components. Instead, they reflect the crossover of the dominance of the transverse cross section to the dominance of the longitudinal cross section. The cross section for ^{14}C represents a situation intermediate to these extremes.

The cross section results for C(p,n) reactions at $E_p = 160$ MeV based on the CKWF (Ref. 3) presented in Figs. 2–5 and Fig. 7 give a reasonable qualitative description of the experimental data, particularly in the large differences in the shapes of the cross section distributions dominated by $p_{1/2} \rightarrow p_{1/2}$ or $p_{1/2} \rightarrow p_{3/2}$ single particle matrix elements. The theoretical results do not give the details of the experimental cross sections for $q \geq 1.2$ fm^{-1}. In the ^{12}C case there is no evidence for the presence of the large contribution from $[LSJ]=[111]$ non-normal parity target densities which peak at $q \simeq 1.2$ fm^{-1}. Small admixtures of $2\hbar\omega$ (or greater) core excitations will appreciably affect the results in this momentum transfer region. This is just the effect considered in the pion condensation precursor studies.[40]

With (p,n) angular distributions covering the range of momentum transfer presented here, there is the likely possibility that one can obtain reasonable quantitative estimates of both the longitudinal and transverse dipole spin transition densities through simultaneous studies of (p,n), (p,p′), and (e,e′) data. The (e,e′) cross sections are independent of $\rho^{s\|}_{11}$.[37,39] The recent work on the IA and GT transition in the (p,n) (Refs. 1, 2, 11, 28, 29, and 37) reaction and on stretched states in (p,n) and (p,p′) (Refs. 37, 39, and 41) have pinned down the properties of the isovector components of the nucleon-nucleon interaction with

some confidence. A study of this type is in progress and will be reported at a later date.

Before leaving this section we make two final comments on the cross sections being considered. First, we note that the nuclei ^{13}C and ^{15}N are similar within the simple shell model. Each has one active particle in the $p_{1/2}$ subshell and the g.s. mirror transitions are mainly $p_{1/2} \rightarrow p_{1/2}$ transitions, consisting of an incoherent sum of F and GT strength. The ^{13}C(p,n)^{13}N(3.51 MeV, $\frac{3}{2}^-$) and the ^{15}N(p,n)^{15}O(6.18 MeV, $\frac{3}{2}^-$) transitions are mainly $p_{1/2} \rightarrow p_{3/2}$ transitions and carry a large fraction of that single particle strength. We compare experimental data for these transitions in Fig. 8. The present data for ^{13}C at 160 MeV are shown in conjunction with a curve indicating the trend of the ^{15}N(p,n)^{15}O data reported by Watson *et al.*[42] at $E_p = 135$ MeV. The two curves for ^{15}N are multiplied by a factor of 0.77 to compensate for the different GT strength values as indicated in Table II. The $p_{1/2} \rightarrow p_{3/2}$ transitions for ^{13}C and ^{15}N in Fig. 8 are almost identical, which is consistent with the theoretical results in Fig. 7. The two $p_{1/2} \rightarrow p_{1/2}$ mirror transitions differ considerably in the region $1.0 \lesssim q \lesssim 1.5$ fm. Specifically, the ^{15}N cross section is about a factor of 1.6 higher than the ^{13}C cross section in this region. Part of this difference is due to the $\Delta J^\pi = 0^+$ (F) components, which are different at the two bombarding energies, $E_p = 135$ and 160 MeV. However, this effect is not that large. The theoretical results in Fig. 7 suggest that there should be a factor of 1.5 difference in the ^{15}N and ^{13}C cross sections at $q \simeq 1.2$ fm^{-1}, so the CKWF provide a good description of the relative magnitudes at large q despite problems with the absolute cross sections. We emphasize that these details are presently not as important as the large qualitative differences between the shapes of the mirror and $p_{1/2} \rightarrow p_{3/2}$ transitions.

D. Analyzing power

In the simple shell model picture, ^{12}C fills the $1p_{3/2}$ subshell, while ^{13}C and ^{14}C have one and two additional neutrons in the $1p_{1/2}$ subshell, respectively. This simple model predicts $B(\mathrm{GT}) = 2.67$ for the ^{12}C(p,n)^{12}N(g.s.) transition (i.e., $p_{3/2} \rightarrow p_{1/2}$); however, the ground state occupation probabilities are altered by the effective $1p$-shell interaction [(8-16)POT] used to construct the CKWF (Ref. 3) that leads to a much reduced value, $B(\mathrm{GT}) = 0.92$. This CKWF value compares quite well with the empirical beta-decay value as shown in Table II. Correspondingly, it was shown in Fig. 2 that the magnitude and shape of the parameter-free DWIA cross section agrees quite well with the (p,n) data up to $q \sim 1.0$ fm^{-1}. On the other hand, the calculated analyzing power has lit-

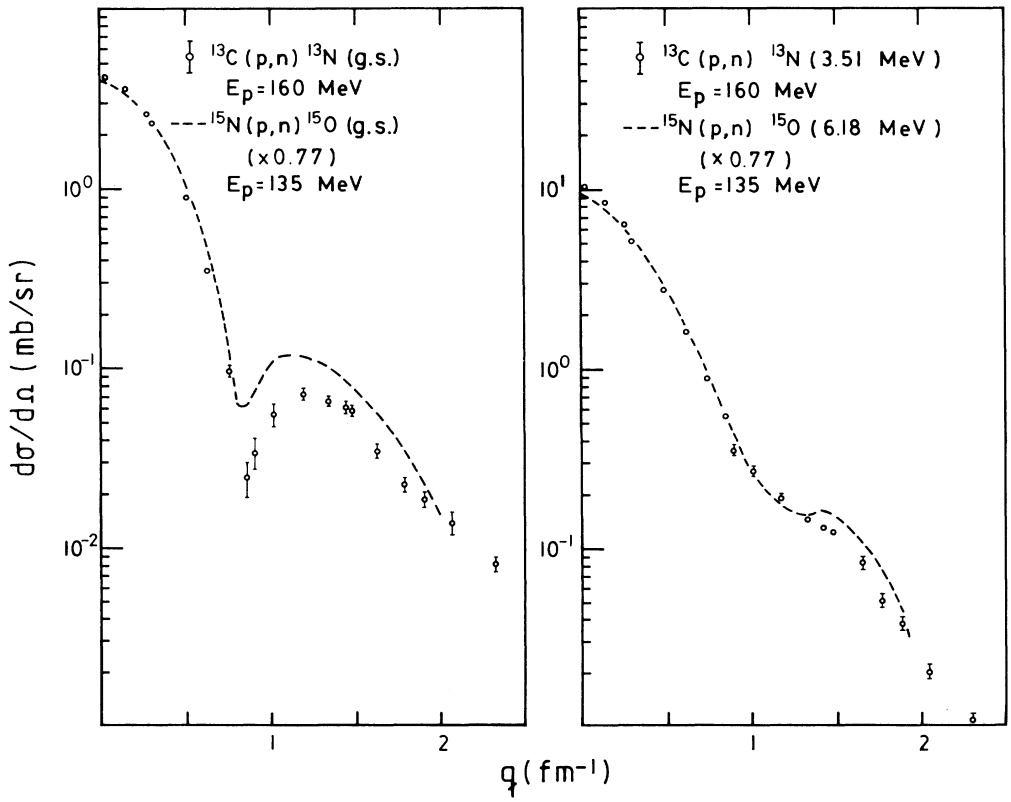

FIG. 8. Data points for the ^{13}C(p,n)^{13}N(g.s.) and (3.51 MeV) angular distribution compared with a normalized empirical curve representing the ^{15}N(p,n)^{15}O(g.s. and 6.18 MeV) transitions. The normalization factor 0.77 corresponds to the ratio of B(GT) strengths.

tle resemblance to the data at all momentum transfers. This has been observed previously in the $^{12}C(\vec{p},p')^{12}C(15.19\ MeV)$ transition studied by Comfort *et al.*[19] at $E_p = 200$ MeV. It was pointed out in Ref. 19 that the calculated analyzing power distribution improved considerably up to $q \sim 1.5$ fm^{-1} if the spectroscopic amplitudes are adjusted to exclude the $[LSJ] = [111]$ nonnormal parity transition densities. These densities contribute because nonlocalities inherent in knock-on exchange and the associated contribution to the nucleon scattering amplitudes are driven primarily by the tensor-exchange interaction. The present calculations for the $^{12}C(p,n)^{12}N(g.s.)$ transition exhibit the same effects (see dashed curve, Fig. 2). Even though the [111] densities are the largest given by CKWF (Ref. 3) for this transition, these contributions to the results for the (p,p') and (p,n) differential cross section are minimal at low q. These densities do not contribute to electromagnetic processes, such as (e,e') reactions, but there are some experiments that provide some measure of these densities (see Refs. 27–30 and discussion in Ref. 19). These densities are likely to be significantly affected by clearly needed core-excitation admixtures in the wave function. An example of this effect for another transition is given in Ref. 38. The particular results presented here depend sensitively on the exchange component of the tensor interaction. Angular distributions of differential cross section and analyzing power extending to large momentum transfer over a range of incident energies provide the database necessary to study these questions.

The analyzing power for the g.s. mirror transition in ^{13}C seems to be dominated by the Fermi amplitude (Fig. 3), the shape of which is qualitatively consistent with the calculations for the ^{14}C IAS transition (Fig. 4). The analyzing power for the 3.51-MeV excitation in $^{13}C(p,n)$ is also qualitatively consistent with the calculations up to $q \leq 1.5$ fm^{-1}. It is interesting that the [111] densities are not important here. The data for the GT transition to the 3.95-MeV state in ^{14}N (Fig. 4) show at $q \sim 1.0$ fm^{-1} an analyzing power larger than that obtained from calculations with the CKWF.[3] This resembles the situation discussed above for mass 12. However, the [111] densities are not as large for this transition in mass 14 (Fig. 7). A DWIA calculation with these densities removed improves the result only slightly. The structure of the cross section minimum in the $^{14}C(p,n)^{14}N(3.95\ MeV)$ reaction is different from that for $^{12}C(p,n)^{12}N(g.s.)$, which is clear from Fig. 7. Since this structure is not perfectly reproduced by the calculations in either case, the analyzing power is subject to related difficulties.

V. SUMMARY

Differential cross section and analyzing power data have been presented for the strongest transitions observed in the (p,n) reaction on carbon isotopes at $E_p = 160$ MeV. DWIA calculations performed using Cohen and Kurath wave functions (CKWF) and the free nucleon-nucleon interaction as parametrized by Franey and Love at $E_p = 175$ MeV are compared with data. The shapes of the calculated differential cross section distributions are in reasonable quantitative agreement with the data for $q \leq 1.2$ fm^{-1} and the qualitative differences in the distributions are well described even at higher q. The forward-angle cross sections for transitions with known $B(GT)$ scale with the beta decay transition strengths, permitting the experimental determination of $B(GT)$ for levels whose beta decay is energetically forbidden. The scale factor required for ^{13}C is different from that for $^{12,14}C$. This effect has been noted in studies of other even and odd isotopes. This indicates a lack of complete understanding of the (p,n) reaction mechanism, but does not affect the empirical extraction of $B(GT)$.

The total observed $B(GT)$ for ^{12}C is in agreement with the predictions of CKWF. For ^{13}C and ^{14}C we obtain the GT quenching factors $Q_{GT} = 0.46$ and 0.60, respectively, when comparing with CKWF. These results are consistent with global values of Q_{GT} presented elsewhere.

The qualitative differences in the shapes of the differential cross section distributions for transitions dominated by $p_{1/2} \rightarrow p_{1/2}$ and $p_{1/2} \rightarrow p_{3/2}$ single particle matrix elements have been discussed in terms of the longitudinal and transverse components of the cross sections. The results based on the CKWF give a qualitative description of the observed phenomena, but fail to give a detailed description of the experimental cross sections and analyzing powers for $q \geq 1.2$ fm^{-1}. The cross section and analyzing power are clearly sensitive to additional core excitation components in the target wave functions in this region of larger momentum transfer. This is an indication of the additional information that can be gained by obtaining angular distributions extending to large momentum transfer for the (p,n) reaction for $E_p \geq 100$ MeV.

This work was supported in part by the National Science Foundation, the U.S. Department of Energy (under Contracts DE-FC05-85ER250000 and DE-AC05-84OR21400), and the Danish Natural Science Research Council.

*Present address: Los Alamos National Laboratory, Los Alamos, NM 87545.

†Supercomputer Computations Research Institute, Florida State University, Tallahassee, FL 32306.

[1] C. D. Goodman *et al.*, Phys. Rev. Lett. **44**, 1755 (1980).

[2] C. Gaarde, J. S. Larsen, and J. Rapaport, in *Spin Excitations in Nuclei*, edited by F. Petrovich *et al.* (Plenum, New York, 1984), p. 65.

[3] S. Cohen and D. Kurath, Nucl. Phys. **73**, 1 (1965); **A101**, 1 (1967); T.-S. H. Lee and D. Kurath, Phys. Rev. C **21**, 293

(1980).
[4]C. A. Goulding *et al.*, Nucl. Phys. **A331**, 29 (1979).
[5]B. D. Anderson *et al.*, Nucl. Instrum. Methods **169**, 153 (1980).
[6]G. L. Moake *et al.*, Phys. Rev. C **21**, 2211 (1980).
[7]J. N. Knudson *et al.*, Phys. Rev. C **22**, 1826 (1980).
[8]J. Rapaport *et al.*, Phys. Rev. C **24**, 335 (1981).
[9]J. Kronenfeld, A. Gal, and J. M. Eisenberg, Nucl. Phys. **A402**, 569 (1983).
[10]T. N. Taddeucci *et al.*, Nucl. Phys. A (in press).
[11]C. D. Goodman *et al.*, Phys. Rev. Lett. **54**, 877 (1985); **54**, 2060(E) (1985).
[12]W. P. Alford *et al.*, Phys. Lett. **179B**, 20 (1986).
[13]N. S. P. King *et al.*, Phys. Lett. **175B**, 279 (1986).
[14]T. N. Taddeucci *et al.*, Phys. Rev. Lett. **52**, 1960 (1984).
[15]C. D. Goodman *et al.*, IEEE Trans. Nucl. Sci. **NS-26**, 2248 (1979).
[16]C. D. Goodman *et al.*, Nucl. Instrum. Methods **151**, 125 (1978); IEEE Trans. Nucl. Sci. **NS-25**, 577 (1978).
[17]C. Gaarde *et al.*, Nucl. Phys. **A369**, 258 (1981).
[18]J. D'Auria *et al.*, Phys. Rev. C **30**, 1999 (1984).
[19]J. R. Comfort *et al.*, Phys. Rev. C **26**, 1800 (1982).
[20]See, for example, F. Petrovich *et al.*, Nucl. Phys. **A383**, 355 (1982).
[21]W. G. Love, in *The (p,n) Reaction and the Nucleon-Nucleon Force*, edited by C. D. Goodman *et al.* (Plenum, New York, 1980), p. 23.
[22]F. Petrovich, *ibid.*, p. 115.
[23]F. Petrovich and W. G. Love, Nucl. Phys. **A354**, 499c (1981).
[24]R. Schaeffer and J. Raynal (unpublished).
[25]J. R. Comfort and B. C. Karp, Phys. Rev. C **21**, 2162 (1980); **22**, 1809(E) (1980).
[26]M. A. Franey and W. G. Love, Phys. Rev. C **31**, 488 (1985).
[27]J. R. Comfort *et al.*, Phys. Rev. C **24**, 1834 (1981); **21**, 2147 (1980), and references therein. Note that the quoted values for the oscillator parameter b do not include the center-of-mass correction factor used here and in Ref. 11.
[28]T. N. Taddeucci *et al.*, Phys. Rev. C **25**, 1094 (1982).
[29]T. N. Taddeucci *et al.*, Nucl. Phys. A (in press); Bull. Am. Phys. Soc. **30**, 1255 (1985).
[30]S. Raman *et al.*, At. Data Nucl. Data Tables **21**, 567 (1978).
[31]F. Ajzenberg-Selove, Nucl. Phys. **A449**, 1 (1986).
[32]D. H. Wilkinson, Nucl. Phys. **A377**, 474 (1982).
[33]S. F. Collins *et al.*, Nucl. Phys. **A380**, 445 (1982).
[34]B. M. Spicer, private communication.
[35]H. O. Meyer *et al.*, Phys. Rev. C **23**, 616 (1981).
[36]F. Petrovich, J. A. Carr, R. J. Philpott, and H. McManus, in *Proceedings of the International Symposium on Electronic Properties of Atomic Nuclei,* edited by H. Horie and H. Ohnuma (Tokyo Institute of Technology, Tokyo, 1984), p. 312.
[37]F. Petrovich, J. A. Carr, and H. McManus, Annu. Rev. Nucl. Part. Sci. **36**, 29 (1986).
[38]F. Petrovich, J. A. Carr, R. J. Philpott, and A. W. Carpenter, submitted to Phys. Rev. Lett.
[39]W. G. Love, M. A. Franey, and F. Petrovich, in Ref. 2, p. 205.
[40]W. Weise and A. Härting, in Ref. 2, p. 173.
[41]R. A. Lindgren and F. Petrovich, in Ref. 2, p. 323.
[42]J. W. Watson *et al.*, Phys. Rev. Lett. **55**, 1369 (1985).